CMS Physics Analysis Summary

Contact: cms-pag-conveners-exotica@cern.ch 2011/10/27

Search for Anomalous Production of Multilepton Events and R-Parity-Violating Supersymmetry in $\sqrt{s} = 7$ TeV pp Collisions

The CMS Collaboration

Abstract

We present a search for anomalous production of events with three or more isolated leptons produced in pp collisions at $\sqrt{s} = 7$ TeV collected by the CMS experiment at the LHC. We analyze 2.1 fb^{-1} of data collected by the CMS experiment during the 2011 LHC run. The search is applicable to any model of new physics that produces multiple leptons. We categorize observed multilepton events into exclusive search channels based on the identity and kinematics of the objects in the events and ordered by the amount of expected standard-model background. We emphasize a data-based estimation of the standard-model backgrounds but also use simulation to estimate some of the backgrounds when appropriate. We interpret search results in the context of R-parity-violating models, for which the presence of missing transverse energy is not guaranteed due to the absence of stable supersymmetric particles. We derive exclusion limits as a function of squark and gluino masses for several R-parity-violating couplings.

1 Introduction

Supersymmetric (SUSY) extensions of the standard model (SM) solve the hierarchy problem and provide a mechanism for unifying particle interactions [1, 2]. Assigning R-parity as $R_\mathrm{p} = (-1)^{3B+L+2s}$, where B and L are baryon and lepton numbers, and s is the particle spin, all SM particle fields have $R_\mathrm{p} = +1$ while all superpartner fields have $R_\mathrm{p} = -1$. In models where R_p is conserved, superpartners can only be produced in pairs, and the lightest superpartner (LSP) is stable and a candidate for a dark matter particle. In addition, R_p conservation ensures proton stability. The role of R-parity in protecting the proton lifetime is an example of a more generalized "matter symmetry," which applies to theories besides SUSY wherein partner particles with differing spins are posited [3].

Models with R-parity-violating (RPV) interactions conserving either B or L in addition to s can avoid direct contradiction with the proton-lifetime upper limits [4]. The most general specification of the superpotential includes three R_p violating terms each parametrized by the Yukawa couplings λ_{ijk}, λ'_{ijk} or λ''_{ijk}.

$$W_{\not R_\mathrm{p}} = \frac{1}{2}\lambda_{ijk}L_iL_j\bar{E}_k + \lambda'_{ijk}L_iQ_j\bar{D}_k + \frac{1}{2}\lambda''_{ijk}\bar{U}_i\bar{D}_j\bar{D}_k,$$

where i, j, and k are generation indices, L and Q are the lepton and quark $SU(2)_L$ doublet superfields and $\bar{E}$, $\bar{D}$, and $\bar{U}$ are the charged lepton, down-like quark, and up-like quark $SU(2)_L$ singlet superfields. The third term violates baryon-number conservation, while the first and second terms are lepton-number violating. In this analysis, we consider leptonic R-parity-violating (L-RPV) models with $\lambda_{ijk} \neq 0$ and $\lambda'_{ijk} = \lambda''_{ijk} = 0$, as well as hadronic R-parity-violating (H-RPV) models with $\lambda_{ijk} = \lambda'_{ijk} = 0$ and $\lambda''_{ijk} \neq 0$. We look for leptons in the final state coming from decays of squarks and gluinos through an intermediate particle, either a neutralino (L-RPV) or bino/higgsino (H-RPV).

If λ_{ijk} is non-zero, the intermediate particle will decay and yield multilepton final states. The value of λ_{ijk} determines the lifetime and therefore the decay length of the intermediate particle, which in our models is the bino. Values of λ_{ijk} considered in this analysis correspond to decay lengths $\lessapprox 100$ μm. Our results are independent of the decay length.

An upper limit on λ_{ijk} is set by constraints from neutrino-mass values. We choose values for λ_{ijk} or λ''_{ijk} that give prompt decay and are consistent with neutrino mass values. In this paper the lepton-generation indices corresponding to e, μ, and τ are sometimes denoted by 1, 2, and 3 respectively.

RPV interactions allow for single production of SUSY particles (sparticles) and for sparticle decay into SM particles only. The decay of the lightest SUSY particle (LSP) results in extra leptons. Due to their clean final-state multilepton signatures, processes with single-slepton production followed by decay to a pair of SM charged leptons are promising search channels for RPV SUSY particles [3]. Prior searches for RPV interactions include those by the CDF and the D0 experiments at the Tevatron [5, 6], which were recently superseded by the Compact Muon Solenoid (CMS) experiment at Large Hadron Collider (LHC) using 35 pb^{-1} of integrated luminosity [7].

Since the LSP is unstable due to RPV, the usual experimental strategy of SUSY searches—selecting events with large missing transverse energy ($E_\mathrm{T}^\mathrm{miss}$)—may not be optimal [3]. We note that the H-RPV events in particular fail to produce sufficient $E_\mathrm{T}^\mathrm{miss}$ in the detector. On the other hand, if the SUSY production is dominated by electroweak processes, the final state

may have minimal hadronic activity. An accident of SUSY mass hierarchy may also suppress hadronic activity despite hadronic production. For example, if the bino mass is just less than that of the squark, the squark production will be effectively captured by the electroweak sector [7]. Searches that require large hadronic activity will thus be insensitive. Motivated by such considerations, we carry out a search for anomalous multilepton production in an inclusive fashion and with minimal reliance on specific kinematic properties. The search findings are then interpreted in the context of RPV models. Specifically, we search for events with three or more isolated (as defined below) final-state leptons. The data used in this analysis correspond to 2.1 fb^{-1} recorded in 2011 with the CMS detector at the LHC running at 7 TeV center-of-mass energy.

2 Detector and Event Trigger

The CMS detector [8] has cylindrical symmetry around the pp beam axis with tracking and muon detectors within pseudorapidity $|\eta| < 2.4$. The tracking system, used to measure the trajectory and momentum of charged particles, consists of multilayered silicon pixel and strip detectors in a 3.8 Tesla solenoidal magnetic field. Particle energies are measured with concentric electromagnetic and hadronic calorimeters. Muon detectors consisting of wire chambers are at the outer radial edge of the detector. Data from pp interactions must satisfy the requirements of a two-level trigger system. The first level performs a fast selection for physics entities above a certain threshold. The second level performs a full event reconstruction.

Electrons are reconstructed as photon-like showers in the electromagnetic calorimeter that are associated with a track. Electrons candidates must satisfy $\Delta\phi$ and $\Delta\eta$ requirements between the shower and the track, and the track must satisfy criteria designed to remove photon conversions in the detector material. Muons are required to have a continuous track through the tracking material and the muon detectors. Muon candidates are also required to be minimum ionizing in the calorimeters.

Data for this search are collected with single- and double-lepton triggers, as well as an electron-muon trigger.

Triggers based on the scalar sum of the transverse momentum of hadronic jets H_{T} are used only for determining lepton-trigger efficiencies. We estimate the efficiency of the single-lepton triggers by selecting isolated leptons in the H_{T} dataset. A single lepton above the p_{T} threshold has a trigger efficiency of $(95.7 \pm 0.7)\%$ and $(92.0 \pm 0.5)\%$ for electrons and muons, respectively. Dilepton triggers have an efficiency of $(99^{+1}_{-2})\%$ for dielectrons, $(92.8 \pm 2.5)\%$ for dimuons, and $(94.8 \pm 3.7)\%$ for the e-μ trigger.

The uncertainties in the efficiencies are largely due to the low statistics of dilepton events in the H_{T}-triggered datasets.

3 Lepton Selection

The signal can contain electrons, muons, and the decay products from taus. In this analysis, we use electrons and muons with $p_{\text{T}} \geq 8$ GeV/c and $|\eta| < 2.1$ which are reconstructed from measured quantities from the tracker, calorimeter, and muon system. Details of reconstruction and identification can be found in Ref. [9] for electrons and in Ref. [10] for muons.

In order to ensure that the trigger efficiency is high and stable for our selected events, we require that each event passing the e-μ trigger have at least one μ and one e with $p_{\text{T}} > 20$ GeV/c

and 10 GeV/c respectively. Events passing the μ-μ trigger are required to have one μ with $p_{\mathrm{T}} > 15$ GeV/c and a second with $p_{\mathrm{T}} > 10$ GeV/c, while those passing the e-e trigger are required to have one e with $p_{\mathrm{T}} > 20$ GeV/c and a second with $p_{\mathrm{T}} > 10$ GeV/c. Single lepton triggers are required to have either a μ with $p_{\mathrm{T}} > 20$ GeV/c or an e with $p_{\mathrm{T}} > 70$ GeV/c.

Taus can decay either leptonically (τ_ℓ) to electrons or muons, or hadronically (τ_{h}). Electrons and muons arising from τ decays are selected as described. The hadronic decays yield either a single charged track (one-prong) or three charged tracks (three-prong) occasionally with additional electromagnetic energy from neutral pion decays. In this analysis, we concentrate on one-prong τ_{h} decay.

Tau leptons are unstable and have decay channels involving leptons and neutrinos, single charged hadrons with or without additional π^0's, and three charged hadrons. The leptonic decays are captured with the electron and muon identification previously defined. For the hadronic decays, we search for candidates with a single charged hadron. Hadronic candidates with one charged and no neutral particles are simply tracks that pass our isolation selection. Hadronic candidates with π^0 are identified using an algorithm in which the invariant mass of the candidates are required to be consistent with τ decays.

To ensure the muon and track candidates are isolated, track p_{T} and calorimeter tower E_{T} in a cone of $\Delta R < 0.3$ around the object are summed and divided by the object's p_{T}. The cone size is extended to 0.4 for electrons. This ratio (I_{rel}) is required to be less than 0.15, which is adequate for selecting electrons, muons, and one-prong τ_{h} decays with no additional neutral pions.

In order to be sensitive to one-prong tau decays accompanied by neutral pions, we reconstruct neutral pions within a cone of $\Delta R < 0.1$ around the isolated track and require the invariant mass of the track and neutral pions to be consistent with that expected from τ_{h} decay. We use the CMS particle-flow algorithm (PFA) [11, 12] to identify the π^0's and to calculate the visible p_{T} of the τ candidate. A requirement on the isolation is imposed as before; however, since neutral pions deposit energy near the charged track, the calorimeter tower E_{T} is summed in an cone of $0.3 > R > 0.1$ around the isolated track. The ratio I_{rel} in this case is the isolation energy divided by the p_{T} of the track and neutral pions and is required to be less than 0.15. All lepton, isolated track, or isolated track with neutral pion candidates are required to originate from the primary vertex and be a distance of $\Delta R > 0.1$ away from other candidates in the event.

In order to estimate the efficiencies of the lepton identification and isolation requirements, we use a tag-and-probe method [13] with $\mathrm{Z} \to \ell^+\ell^-$ events. We find that the simulation models the efficiencies correctly to within $\pm 1\%$ ($\pm 2\%$) for muons (electrons). We estimate the efficiency for an isolated track and isolated track with neutral pions by comparing the number of $\mathrm{Z} \to \tau_\mu \tau_{\mathrm{h}}$ events in simulation to data. We measure a ratio of the data efficiency to the simulation efficiency for single-prong taus of 1.02 ± 0.04.

4 Search Strategy

We select events with either three or four isolated objects (electrons, muons, or τ_h) and then categorize them based on the number of Drell-Yan-like opposite-sign, same-flavor (OSSF) lepton pairs N_{DY} and whether or not the event passes a Z-veto (ZV) by containing no OSSF lepton pairs with invariant mass between 75 and 105 GeV/c^2 [7].

Events with an OSSF lepton-pair mass below 12 GeV/c^2 are rejected to exclude events with J/Ψ, Υ, low-mass Drell-Yan processes, as well as photon conversions.

We use PFA-reconstructed jets [14] with $|\eta| < 2.5$ and $p_T > 40$ GeV/c. Jets are required to be have a distance $\Delta R > 0.30$ from any isolated electron, muon, or track. We define S_T as the scalar sum of E_T^{miss}, H_T, and the p_T of all isolated leptons and τs.

The S_T distribution peaks near the sum of the parent particle masses if most of the energy is reconstructed as leptons, jets, or E_T^{miss}; therefore, signal events generated by heavy particles are expected to have much larger S_T than SM backgrounds. We further classify events into three categories of S_T value: low ($S_T < 300$ GeV), medium ($300 < S_T < 600$ GeV), and high ($S_T > 600$ GeV). New-physics scenarios involving H-RPV or L-RPV both have S_T well above 600 GeV, although the relative contributions to S_T from E_T^{miss}, jets, and leptons differ.

5 Backgrounds and Systematic Uncertainties

Several SM sources can produce signatures that mimic our signal. The largest background remaining after the basic three-lepton reconstruction originates from the Z+jets process (including Drell-Yan production), in which the Z boson decays leptonically and a third lepton is produced from a jet or a photon. The probability for a jet to produce an isolated lepton candidate depends on many factors, including the type of jet, the p_T spectrum, and the multiplicity of jets in the event. Many of these factors may be inaccurately modeled in the simulation. Therefore we estimate the background from jets with dilepton data. We relate the rate for jets to produce isolated-lepton candidates to the rate for jets to produce isolated tracks (from $K^{\pm}$ or $\pi^{\pm}$). We use events with two leptons and an isolated track to determine the number of three-lepton events where one lepton was misidentified as isolated. Similarly, we use the number of events with two leptons and two isolated tracks to determine the number of four-lepton events in which two leptons were misidentified as isolated.

The ratio of isolated-lepton rates to isolated-track rates is determined using jet-triggered data. The ratio of these rates is sensitive to the abundance of heavy-flavor jets in the events. To test for variation in the abundance of heavy-flavor jets we study the impact-parameter distribution of non-isolated tracks. The ratio of the number of isolated leptons from jets to isolated tracks from jets in dilepton data is found to be $(1.4 \pm 0.2)\%$ and $(1.1 \pm 0.2)\%$ for muons and electrons, respectively, after contributions from dileptonic decays of $t\bar{t}$ are removed. The systematic uncertainties on these ratios come from the difference in jet properties between the QCD and dilepton samples.

For channels with τ_h, we extrapolate the isolation sideband $0.2 < I_{rel} < 1.0$ to the signal region $I_{rel} < 0.15$. The ratio of the number of isolated tracks in the two regions is $(15 \pm 3)\%$. We study the variation of this ratio for a number of QCD samples and assign a 30% systematic uncertainty for it. The ratio is applied to the dilepton event sample.

We find simulation to be adequate for estimating backgrounds from the following processes: $ZZ \to 4\ell$, $W^{\pm}Z \to 3\ell$, and $t\bar{t}$+jets $\to 2\ell$.

In order to demonstrate the adequacy of $t\bar{t}$ simulation, we compare data and simulations for distributions related to these processes. An example is the S_T distribution for two control datasets: a single-lepton dataset with an isolated muon and a jet originiating from a b-quark; and a dilepton dataset with both an isolated muon and an isolated electron. These datasets are dominated by $t\bar{t}$ events for large S_T. Figure 1 shows good agreement between the S_T distributions in the data and simulation for both datasets.

Asymmetric conversions—a process whereby one lepton takes most of the photon energy and the second lepton is very soft and not measured—can be a significant source of background.

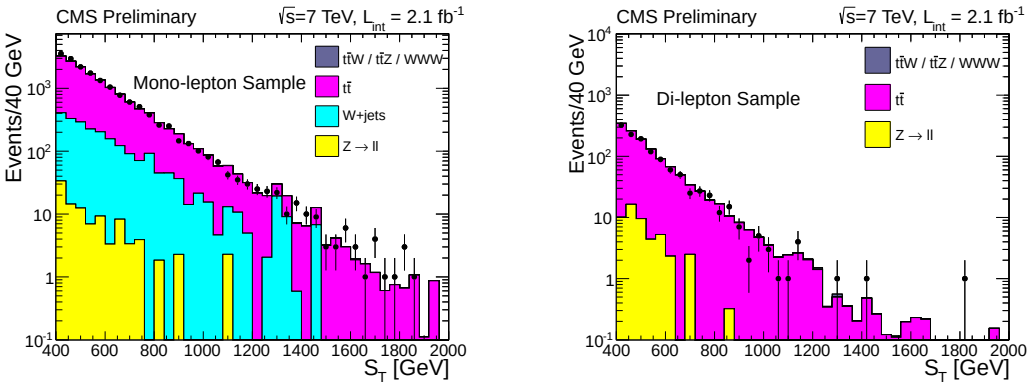

Figure 1: A comparison of data and simulation for the S_T distribution in datasets dominated by $t\bar{t}$. The single-lepton dataset is shown on the left, and the dilepton dataset is shown on the right.

There are two different types of photon conversions that give rise to backgrounds in multi-lepton analyses. The first type is an external conversion in which a photon radiated by the collision interacts with detector material and produces an $\ell^+\ell^-$ pair (primarily e^+e^- pairs, but very rarely $\mu^+\mu^-$ pairs). The electron-identification requirements strongly suppress external conversions. The second type of conversion is an internal photon conversion, where the photon is virtual and does not interact with the detector. Internal photon conversions can produce muons almost as often as electrons and can occur in any process that produces photons.

Internal conversions may not be properly simulated by the MC due to low-energy cutoffs for emitted leptons; instead, we use data-driven methods to estimate this background. We assume that the rate for standard-model processes to produce on-shell photons is proportional to the rate for producing virtual photons that yield asymmetric conversions. This is justified by the fact that off-shell photons are dominated by the low mass end of the spectrum, which have kinematics that are very similar to real photons. Furthermore, this method essentially compares the integral of the cross section over two different regions of phase space. The conversion rate for producing a signal lepton via radiation is a ratio of the probability for a photon to produce a valid lepton candidate via asymmetric conversion to the probability for an on-shell photon to pass all selection criteria.

For this analysis, the most important source of photon-conversion background involves Z bosons decaying to leptons, and an asymmetric internal conversion of a γ^* from one of the Z's decay leptons. The invariant mass of the leptons from the Z decay might not reconstruct at the Z-pole, and the asymmetric internal conversion would add one more lepton to the event.

We find clean FSR events by examining 3-body masses on the Z peak. The ratio of the number of $\ell^+\ell^-\ell^\pm$ to $\ell^+\ell^-\gamma$ on the Z peak gives conversion factor for muons (C_μ) of $(0.4 \pm 0.1)\%$ and for electrons (C_e) of $(1.1 \pm 0.2)\%$, where only statistical uncertainties are given. We assign an additional systematic uncertainty of 100% to these conversion factors due to our underlying assumption that the number of isolated photons is proportional to the number of leptons from asymmetric internal and external conversions. We use these conversion factors to estimate the background due to asymmetric conversions.

We assign a systematic uncertainty for the luminosity of 4.5%, which is correlated between all signal channels and the background estimates which are scaled from simulations. Uncertainties on lepton identification and trigger efficiencies discussed above also contribute to the systematic uncertainty in the result. The uncertainty on the $t\bar{t}$ background estimate contributes

Source of Uncertainty	Uncertainty
Luminosity	4.5%
PDF	14%
Renormalization Scale	10%
Muon ID	0.1 %
Electron ID	0.3%
τ ID	3.7 %
Muon isolation at 8 (100) GeV/c	11% (0.2%)
Electron isolation at 8 (100) GeV/c	14% (0.6%)
Single Muon trigger efficiency	0.5%
Single Electron trigger efficiency	0.7%
Double Muon trigger efficiency	2.5%
Double Electron trigger efficiency	2%
Electron-Muon trigger efficiency	3.7%
$t\bar{t}$ background	50%
WZ background	40%
ZZ background	40%

Table 1: The sources of systematic uncertainties associated with this analysis. Note that the magnitudes of uncertainties listed above do not have proportionate impact on the results as given in various tables and figures.

a large systematic uncertainty in channels where this process is prominent.

We summarize all of the systematic uncertainties in Table 1. The systematic uncertainty on the $t\bar{t}$ cross section dominates the background uncertainties for the three-lepton channels. The size of this uncertainty is governed by the limited statistics of the top-enriched control sample used to measure the isolation efficiency of μ and e from b-jets in data.

6 Results

Table 2 shows the number of observed events, and that expected from the standard model. Results for a total of 54 channels with varying levels of SM background are listed. The rows indicate the total number of isolated leptons in the event whereas the columns indicate how many of those leptons are τ candidates. Note that the level of background increases from top to bottom since the most unlikely configurations are at the top and the most common ones are at the bottom. Reflecting the difficulty of tau reconstruction, the background is also seen to increase from left to right. The background estimation for all channels is performed in a uniform manner using the methods and sources described above.

The observations and SM expectations agree within uncertainties for most channels. We note that the large multiplicity of exclusive channels in this analysis makes assigning a significance to any particular excess somewhat subjective.

We observe one four-lepton high-S_T event in a bin with a low SM-background expectation. We find that the dominant SM contribution to the bin is from di-Z production, where one of the Z bosons is off-shell. The background estimate is calculated with MADGRAPH [15], and an uncertainty of 40% is assigned based on differences in the estimate with MCFM [16]. Consistent predictions in low S_T and on-shell control samples of the data are found; however, data is not available with which to test the MC prediction for off-shell diboson production at high S_T.

We apply our search findings to RPV models in which either λ_{122} , λ_{123}, or λ_{233} couplings are non-zero. In the specific slepton co-NLSP RPV SUSY topology utilized here (see Ref. [7] and references therein) the bino is the lightest superpartner with a fixed mass of 300 GeV/c^2. The gluino and degenerate squark masses, m_{gluino} and m_{squark}, are variable and define the parameter space for our search. All other superpartners are decoupled, holding the bino RPV decay width fixed. Table 2 also shows the expectation from two specific L-RPV mass spectra and couplings. One is with a λ_{122} coupling for squark and gluino masses of 1100 GeV/c^2 and 1000 GeV/c^2, while the second is richer in τ content due to its λ_{123} coupling and has 1000 GeV/c^2 and 1100 GeV/c^2 masses, respectively.

In order to determine the sensitivity for various signal-model scenarios, we perform a simultaneous fit across *all* the exclusive channels listed in the table to compute the likelihood of observing a signal.

Simulations for the three separate L-RPV models and the one H-RPV model are generated in a grid in the squark–gluino mass plane, and used to calculate the signal strengths in different channels. We determine the exclusion limit for these channels using a method based on Bayesian inference. We use a multi-channel fitting procedure which models the number of events in each channel as a Poisson distribution with expected and observed values. A flat prior is assumed for the signal strength, and the nuisance parameters (associated with the systematic uncertainties) are modeled with log-normal distributions. Using the results for observed and expected exclusion fits, we are able to find curves that represent which region of the plane is excluded at 95% confidence level (C.L.) for each of the models.

In Fig. 2, we show the 95% C.L. exclusion-limit contours for λ_{122}, λ_{123}, λ_{233} and H-RPV couplings in the MSSM parameter space of m_{squark} versus m_{gluino}, along with the expected limits in the absence of signal. We note that the limits for the tau cases would be weaker in absence of the strategy to retain high-background channels. In the H-RPV case, gluino masses below 500 GeV/c^2 are not excluded even though the production cross section in this region can be large. This is due to the reduced gluino branching fraction to the bino and subsequently to leptons.

Table 2 illustrates a key feature of this analysis: the division into exclusive channels, some with large SM expectations and some where it is negligible. Any specific new-physics model may produce excess events in a subset of channels, and not in others. The former constitute the "signal" regions for that particular model, while the latter make up the "control" regions. The sensitivity of this analysis to a given model depends on the size of the contribution to channels with low SM expectations.

We have performed a search for physics beyond the SM using a variety of multilepton final states. We see good agreement between observations and expectations in channels with large SM expectations both on-Z and off-Z. By studying many channels with different requirements, the search maximizes sensitivity to new physics. We demonstrate the reach of the search by applying the results to the case of R-parity-violating decays of SUSY particles in multilepton events. We are able to exclude R-parity-violating couplings λ_{122}, λ_{123} and λ_{233} and H-RPV for squark and gluino masses in the 1 TeV/c^2 range. The 95% C.L. exclusions on λ_{122} and λ_{123} presented here significantly exceed those from our prior search using 35 pb^{-1} [7]. We have also presented the more difficult-to-achieve exclusions for the τ-dominated λ_{233} RPV coupling for the first time.

Table 2: Number of events observed in 2.1 fb^{-1} data (obs), the SM expectation, and expected event counts from typical signals: The rows indicate the *total* number of isolated leptons in the event. The columns indicate the number of τ's among the isolated objects. The number of Drell-Yan pairs is specified by DYn; the S_{T} ranges in GeV are Low (< 300 GeV), Mid ($300 < S_{\mathrm{T}} < 600$ GeV), and High (> 600 GeV); and ZV stands for Z-Veto, indicating there are no OSSF lepton pairs with invariant mass in the Z window. For example, the entry in row marked "3 (DY1)S_{T}(Mid)" and column marked "τ=1" would be the number of three lepton events which have one opposite-sign electron or muon (same flavor) pair in it, one tau candidate and the total event S_{T} in the 300 to 600 GeV range. The channel right above it requires a Z-veto in addition, and thus suffers from significantly less background. The channels are exclusive, i.e., non-overlapping. The column labeled sigA is for the L-RPV signal with λ_{122} coupling for squark and gluino masses of 1100 GeV/c^2 and 1000 GeV/c^2, while the column labled sigB is for λ_{123}, 1000 GeV/c^2 and 1100 GeV/c^2, respectively. Note the shift in signal between τ=0 and τ=1 channels because λ_{123} is tau rich. The totals at the bottom are for informational purposes.

# Bodies (Selection)	τ=0				τ=1				τ=2			
	obs	SM	sigA	sigB	obs	SM	sigA	sigB	obs	SM	sigA	sigB
$\geq$ FOUR Lepton Results												
4 (DY0) S_{T}(High)	0	0.0000 ± 0.0007	2.9	0.3	0	0.00 ± 0.09	2.0	2.5	0	0.09 ± 0.07	0.5	7.0
4 (DY0) S_{T}(Mid)	0	0.001 ± 0.002	0.0	0.0	0	0.11 ± 0.10	0.0	0.0	0	0.68 ± 0.30	0.0	0.0
4 (DY0) S_{T}(Low)	0	0.02 ± 0.02	0.0	0.0	0	1.69 ± 0.27	0.0	0.0	4	1.34 ± 0.41	0.0	0.0
4 (DY1,ZV) S_{T}(High)	1	0.002 ± 0.001	12.6	1.1	0	0.02 ± 0.07	6.1	5.5	0	0.10 ± 0.07	0.7	2.4
4 (DY1) S_{T}(High)	1	0.010 ± 0.004	2.9	0.4	0	0.22 ± 0.10	1.6	1.8	0	0.15 ± 0.07	0.0	0.3
4 (DY1,ZV) S_{T}(Mid)	0	0.008 ± 0.003	0.0	0.0	0	0.20 ± 0.09	0.0	0.0	0	0.45 ± 0.19	0.0	0.0
4 (DY1) S_{T}(Mid)	0	0.27 ± 0.11	0.0	0.0	2	1.38 ± 0.38	0.0	0.0	2	1.52 ± 0.44	0.0	0.0
4 (DY1,ZV) S_{T}(Low)	0	0.03 ± 0.01	0.0	0.0	4	2.2 ± 1.4	0.0	0.0	10	10.0 ± 7.8	0.0	0.0
4 (DY1) S_{T}(Low)	0	0.37 ± 0.13	0.0	0.0	14	6.6 ± 1.5	0.0	0.0	56	30 ± 22	0.0	0.0
4 (DY2,ZV) S_{T}(High)	0	0.005 ± 0.002	7.7	0.8	–	–	–	–	–	–	–	–
4 (DY2) S_{T}(High)	0	0.33 ± 0.13	3.9	0.5	–	–	–	–	–	–	–	–
4 (DY2,ZV) S_{T}(Mid)	0	0.022 ± 0.009	0.0	0.0	–	–	–	–	–	–	–	–
4 (DY2) S_{T}(Mid)	1	2.2 ± 0.9	0.0	0.0	–	–	–	–	–	–	–	–
4 (DY2,ZV) S_{T}(Low)	0	0.04 ± 0.02	0.0	0.0	–	–	–	–	–	–	–	–
4 (DY2) S_{T}(Low)	10	7.2 ± 2.9	0.0	0.0	–	–	–	–	–	–	–	–
THREE Lepton Results												
3 (DY0) S_{T}(High)	2	0.53 ± 0.25	6.3	3.2	10	5.5 ± 1.9	4.0	18.6	10	15.5 ± 3.6	0.5	6.6
3 (DY0) S_{T}(Mid)	3	3.8 ± 1.5	0.0	0.0	63	45 ± 15	0.0	0.0	106	114 ± 16	0.0	0.0
3 (DY0) S_{T}(Low)	9	6.4 ± 2.0	0.0	0.0	291	236 ± 42	0.0	0.0	1590	2054 ± 404	0.0	0.0
3 (DY1,ZV) S_{T}(High)	4	1.34 ± 0.40	19.9	8.4	5	8.8 ± 1.6	2.7	8.0	–	–	–	–
3 (DY1) S_{T}(High)	8	7.9 ± 2.6	3.2	2.4	21	18.5 ± 2.7	0.3	0.7	–	–	–	–
3 (DY1,ZV) S_{T}(Mid)	20	10.2 ± 2.8	0.0	0.0	71	64 ± 12	0.0	0.0	–	–	–	–
3 (DY1) S_{T}(Mid)	31	43 ± 13	0.0	0.0	216	222 ± 23	0.0	0.0	–	–	–	–
3 (DY1,ZV) S_{T}(Low)	88	85 ± 21	0.0	0.0	2579	2004 ± 441	0.0	0.0	–	–	–	–
3 (DY1) S_{T}(Low)	368	381 ± 92	0.0	0.0	9611	7839 ± 1725	0.0	0.0	–	–	–	–
Totals	546	549 ± 95	59.0	17.0	12887	10456 ± 1781	17.0	37.0	1778	2228 ± 405	2.0	16.0
Totals 4L	13	10.4 ± 3.1	29.9	3.1	20	12.4 ± 2.1	9.7	9.8	72	44 ± 23	1.0	10.0
Totals 3L	533	539 ± 95	29.0	14.0	12867	10443 ± 1781	7.0	27.0	1706	2184 ± 404	0.0	7.0

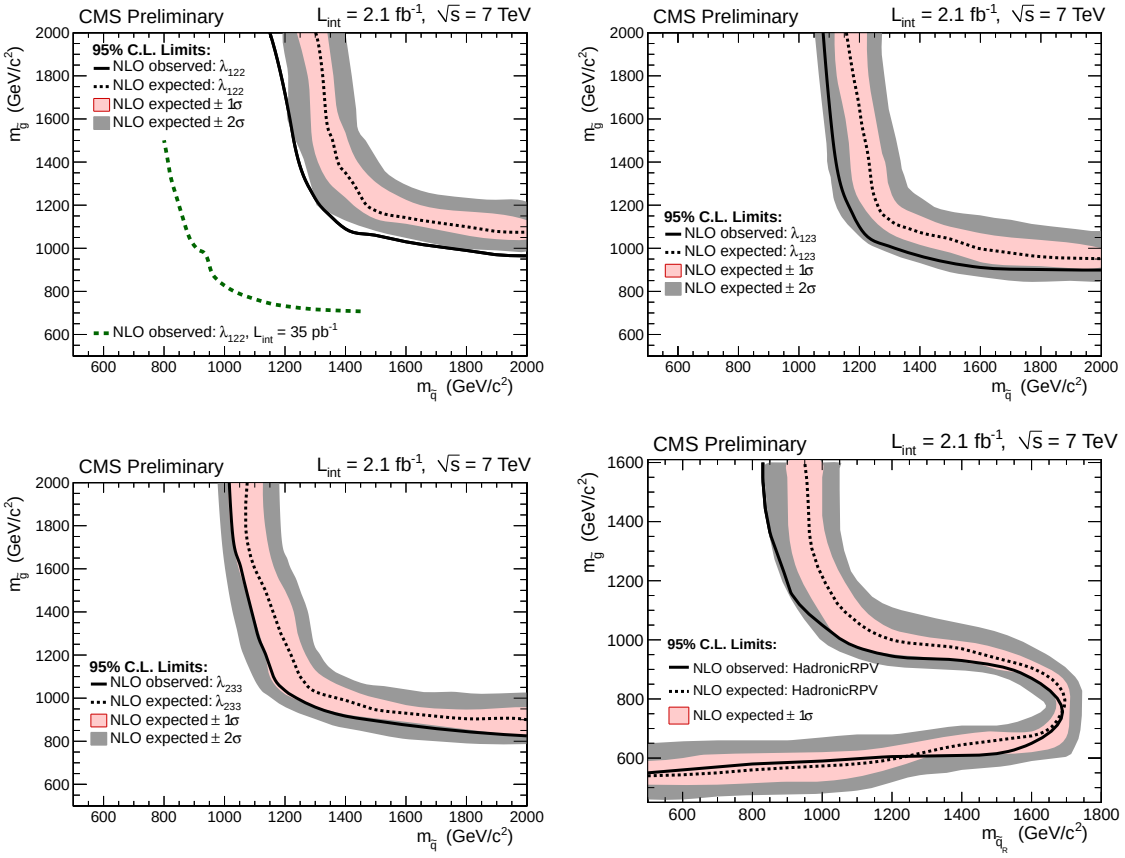

Figure 2: 95% C.L. limits for RPV couplings λ_{122}, λ_{123}, λ_{233} and Hadronic-RPV scenarios as a function of the squark and gluino masses for a SUSY topology described in the text. The observed limits, along with limits expected in the absence of signal are shown, along with the uncertainty in the expectation. Masses to the left of the curves are excluded. For the H-RPV scenario gluino masses below ~ 500 GeV/c^2 are allowed for reasons explained in the text. The previous limit on λ_{122}, obtained with 35 pb^{-1}, is shown as a dotted line on the left plot.

References

[1] H. P. Nilles, "Supersymmetry, Supergravity and Particle Physics", *Phys. Rept.* **110** (1984) 1. doi:10.1016/0370-1573(84)90008-5.

[2] H. E. Haber and G. L. Kane, "The Search for Supersymmetry: Probing Physics Beyond the Standard Model", *Phys. Rept.* **117** (1985) 75. doi:10.1016/0370-1573(85)90051-1.

[3] R. Barbier et al., "R-parity violating supersymmetry", *Phys. Rept.* **420** (2005) 1–202, arXiv:hep-ph/0406039. doi:10.1016/j.physrep.2005.08.006.

[4] Particle Data Group Collaboration, "Review of particle physics", *J. Phys.* **G37** (2010) 075021. doi:10.1088/0954-3899/37/7A/075021.

[5] D0 Collaboration, "Search for R-parity violating supersymmetry via the $LL\overline{E}$ couplings λ_{121}, λ_{122} or λ_{133} in $p\bar{p}$ collisions at $\sqrt{s}$ = 1.96-TeV", *Phys. Lett.* **B638** (2006) 441. doi:10.1016/j.physletb.2006.05.077.

[6] CDF Collaboration, "Search for anomalous production of multilepton events in $p\bar{p}$ collisions at $\sqrt{s}$ = 1.96-TeV", *Phys. Rev. Lett.* **98** (2007) 131804. doi:10.1103/PhysRevLett.98.131804.

[7] CMS Collaboration, "Search for Physics Beyond the Standard Model Using Multilepton Signatures in pp Collisions at sqrt(s)=7 TeV", arXiv:1106.0933.

[8] CMS Collaboration, "The CMS experiment at the CERN LHC", *JINST* **0803** (2008) S08004. doi:10.1088/1748-0221/3/08/S08004.

[9] CMS Collaboration, "Electron reconstruction and identification at $\sqrt{s}$ = 7 TeV", *CMS Physics Analysis Summary* **CMS-PAS-EGM-10-004** (2010).

[10] CMS Collaboration, "Performance of muon identification in pp collisions at $\sqrt{s}$ = 7 TeV", *CMS Physics Analysis Summary* **CMS-PAS-MUO-10-002** (2010).

[11] CMS Collaboration, "Study of tau reconstruction algorithms using pp collisions data collected at $\sqrt{s}$ = 7 TeV", *CMS Physics Analysis Summary* **CMS-PAS-PFT-10-004** (2010).

[12] CMS Collaboration, "CMS Strategies for tau reconstruction and identification using particle-flow techniques", *CMS Physics Analysis Summary* **CMS-PAS-PFT-08-001** (2010).

[13] CMS Collaboration, "Measurement of the Inclusive W and Z Production Cross Sections in pp Collisions at sqrt(s) = 7 TeV", arXiv:1107.4789.

[14] CMS Collaboration, "Commissioning of the Particle-Flow Reconstruction in Minimum-Bias and Jet Events from pp Collisions at 7 TeV", *CMS Physics Analysis Summary* **CMS-PAS-PFT-10-002** (2010).

[15] J. Alwall, M. Herquet, F. Maltoni et al., "MadGraph 5 : Going Beyond", *JHEP* **1106** (2011) 128, arXiv:1106.0522. * Temporary entry *. doi:10.1007/JHEP06(2011)128.

[16] J. M. Campbell, R. Ellis, and C. Williams, "Vector boson pair production at the LHC", *JHEP* **1107** (2011) 018, arXiv:1105.0020. doi:10.1007/JHEP07(2011)018.

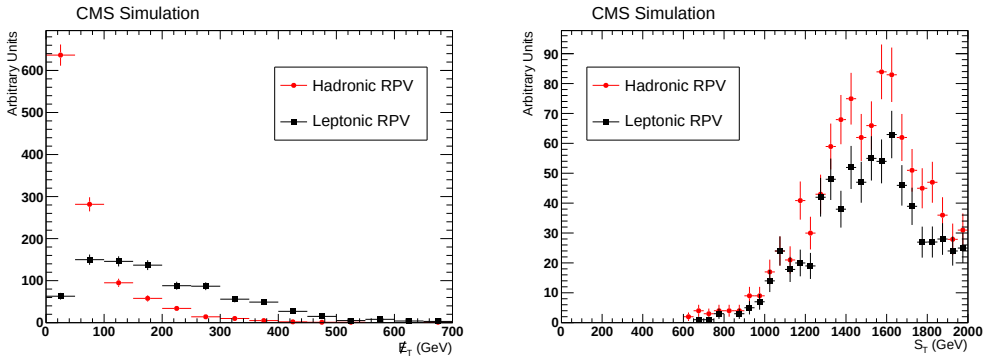

Figure 3: The $E_{\mathrm{T}}^{\mathrm{miss}}$ and S_{T} distributions for L-RPV and H-RPV models. Note that a requirement on S_{T} preserves both types of signal, while $E_{\mathrm{T}}^{\mathrm{miss}}$ does not.

A APPENDIX

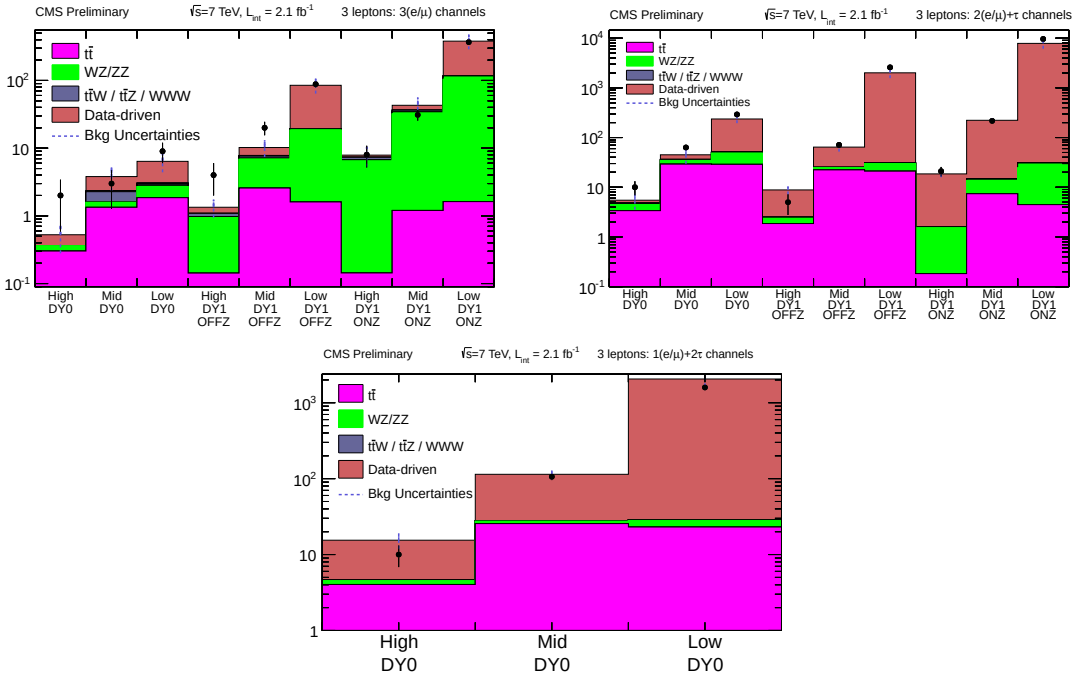

Figure 4: Observed signal (dots) and SM backgrounds (histogram) for various three-lepton channels described in the text.

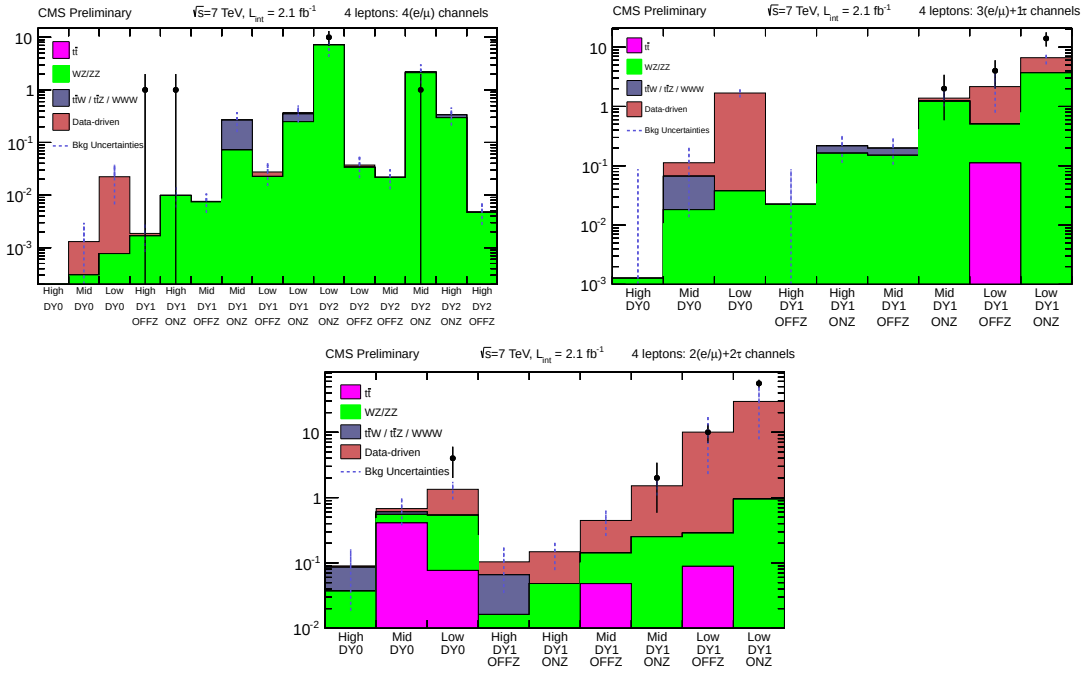

Figure 5: Observed signal (dots) and SM backgrounds (histogram) for various four-lepton channels described in the text.

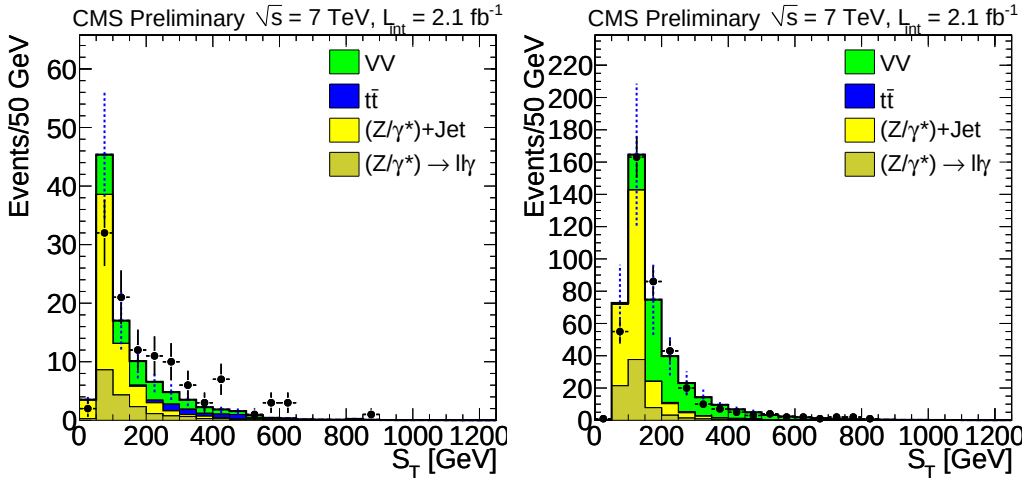

Figure 6: The S_T distributions for three-lepton events passing all selection criteria for the three lepton, no-τ channel, except S_T. Observed events (dots) and expected SM background (histogram) are shown. Plots on the left have the Z-veto applied, while plots on the right include leptons from Z decays.

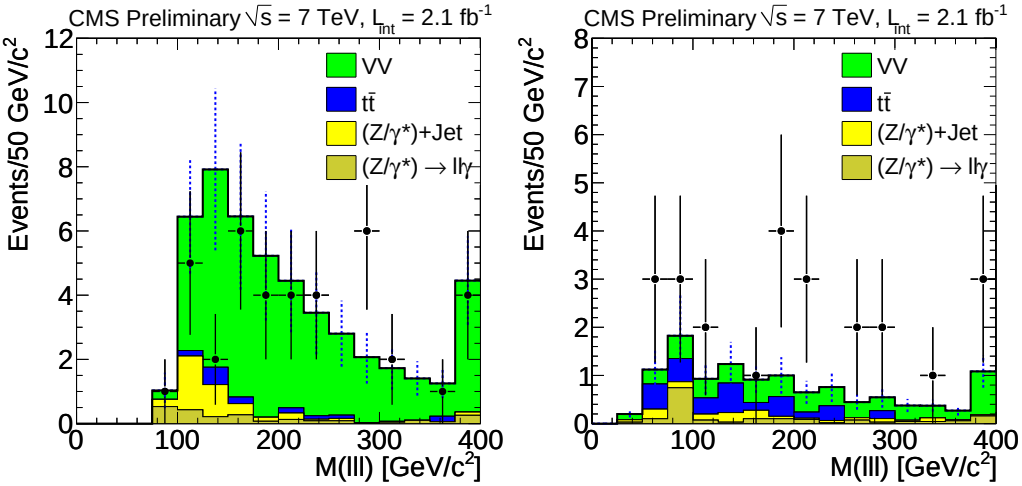

Figure 7: The $m_{\ell^+\ell^-\ell^\pm}$ distributions for three-lepton events passing all selection criteria for the three lepton, no-τ channel, with $S_T > 300$ GeV. Observed events (dots) and expected SM background (histogram) are shown. Plots on the left have the Z-veto applied, while plots on the right include leptons from Z decays.

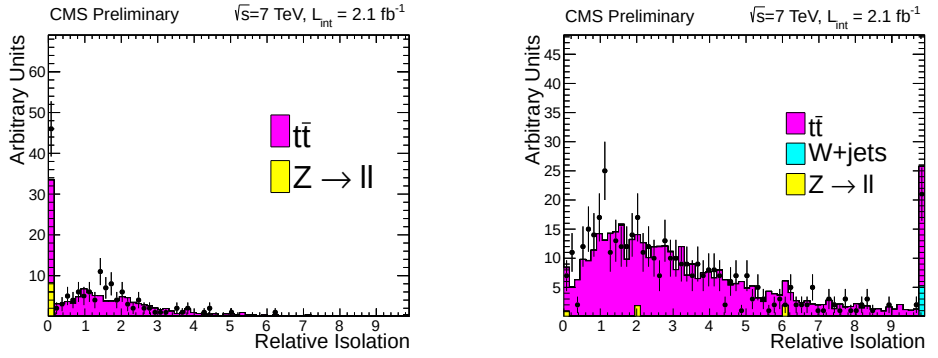

Figure 8: The isolation distributions of leptons with large impact parameter ($d_{xy} > 0.02$ cm, primarily from jets) in a data sample composed predominantly of $t\bar{t} \to \ell^{\circ} b\bar{b}jj$. The plot on the right is for electrons, the one on the left for muons.

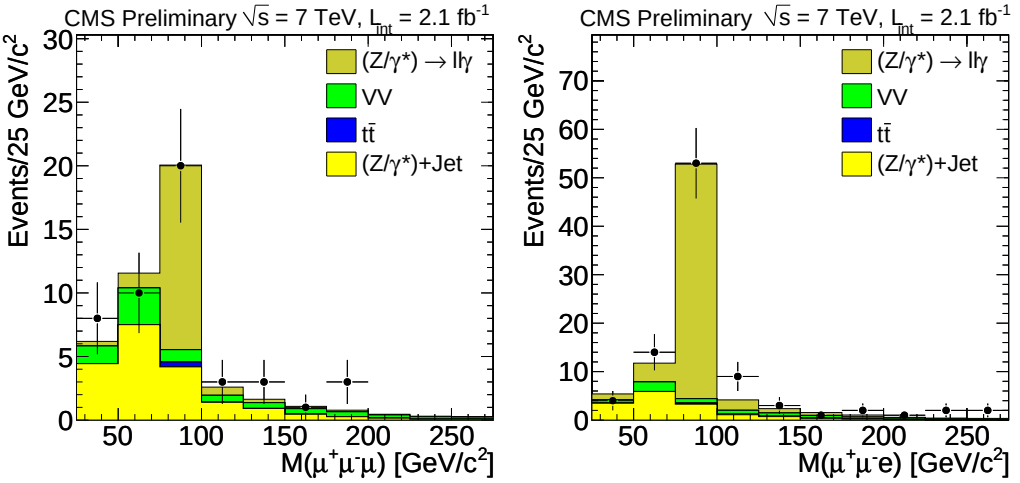

Figure 9: Invariant mass of 3μ and $\mu\mu e$, showing clear Z-peaks, due to the asymmetric conversion background discussed in the text.

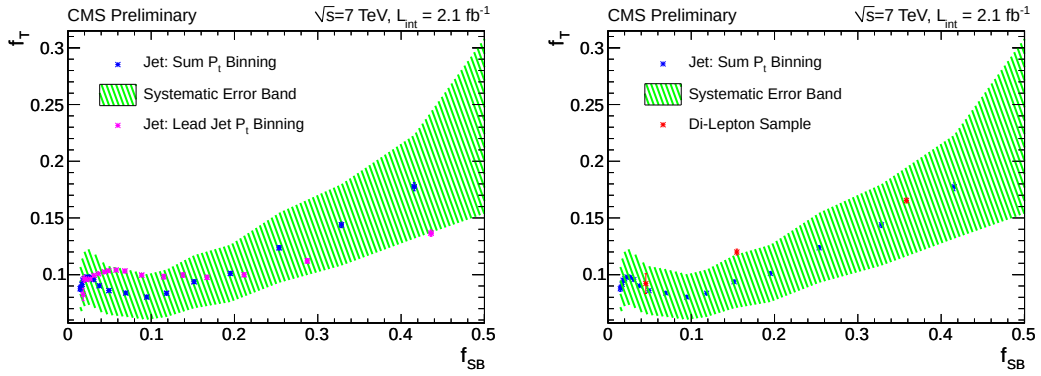

Figure 10: f_t vs f_{SB} for Isolated Tracks (Taus with no π^0s) with Visible Tau P_t between 8–24 GeV; and Comparison with DiLepton Data.

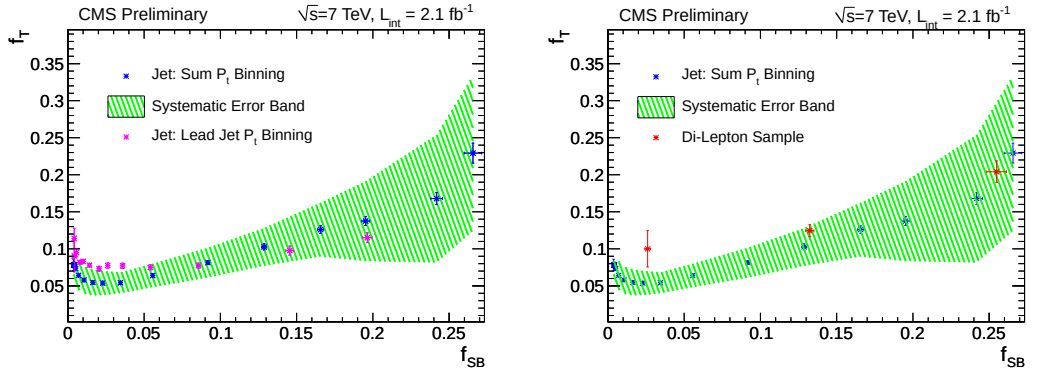

Figure 11: f_t vs f_{SB} for Isolated Tracks (Taus with no π^0s) with Visible Tau P_t between 24–48 GeV; and Comparison with DiLepton Data.

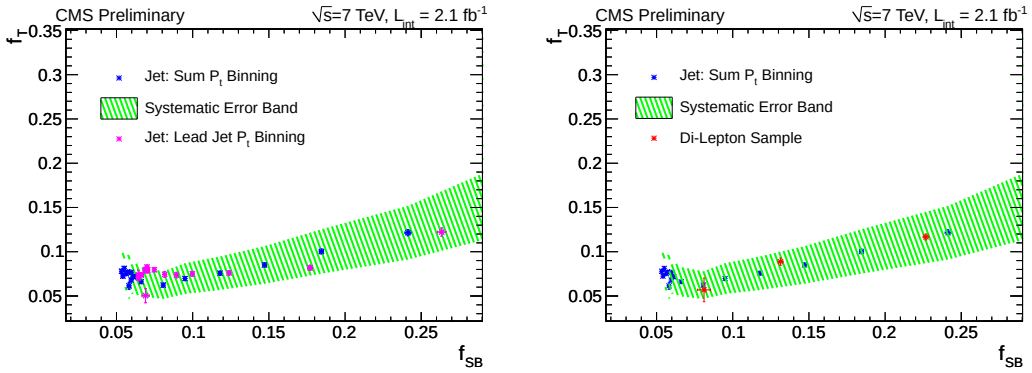

Figure 12: f_t vs f_{SB} for 1-prong Taus with π^0s and Visible Tau P_t between 15–24 GeV; and Comparison with DiLepton Data.

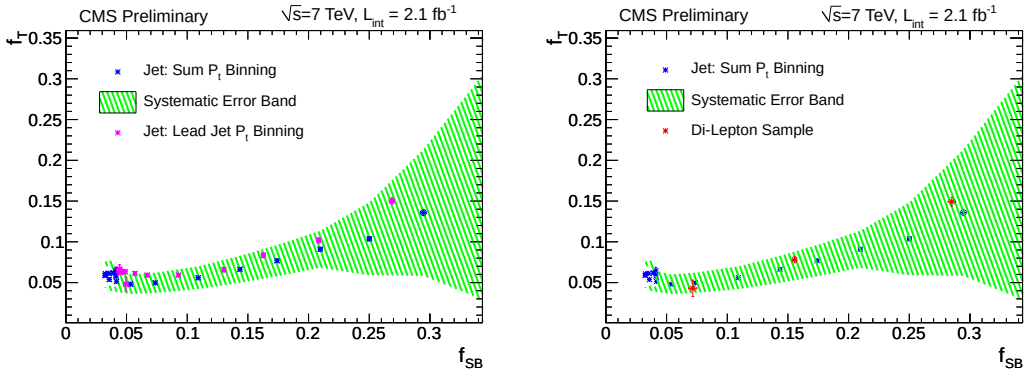

Figure 13: f_t vs f_{SB} for 1-prong Taus with π^0s and Visible Tau P_t between 24–48 GeV; and Comparison with DiLepton Data.

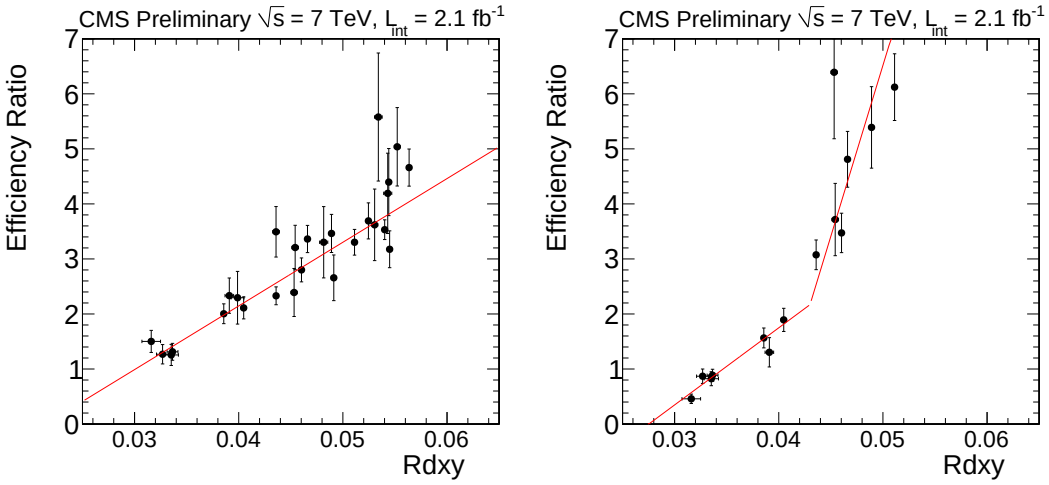

Figure 14: Efficiency ratio of leptons to tracks versus fraction of non-isolated tracks with a large impact parameter. The efficiency ratio for muons is left and electrons is right.